CellPress
OPEN ACCESS

Trends in
Biotechnology

Research Article

Acetogenesis to ethanologenesis: facilitating NADH oxidation via reductive acetate uptake

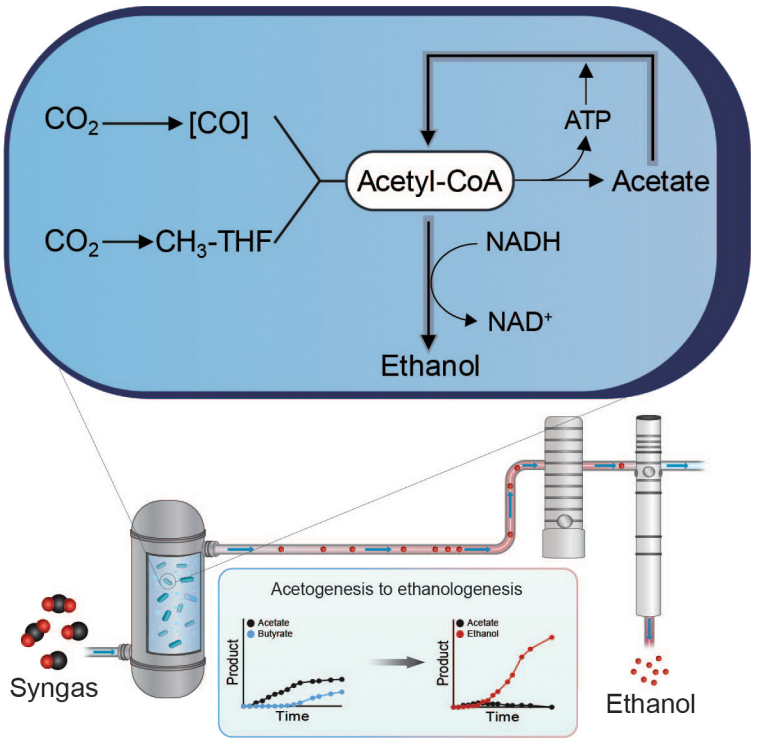

Acetate is not always an end product in acetogenesis. This study identified butyrate production with acetate uptake, a finding that led to the development of a strain for ethanol production with complete acetate uptake. The shift from acetogenesis to ethanologenesis could reduce operating costs in downstream processed for commercial synthetic gas (syngas) fermentation.

Soyoung Oh, Jiyeong Jeong, Byeonghyeok Park, Byeongchan Kang, Ji-Yeon Kim, Sehoon Park, Dong-Hun Lee, Seunghyeon Jung, Mungyu Lee, Wonjung Lee, Muhammad Yasin, Junhyeok Seo, Zee-Yong Park, Kyung-Hoon Shin, Volker Müller, In-Geol Choi, In Seop Chang

igchoi@korea.ac.kr (I.-G. Choi)
ischang@gist.ac.kr (I.S. Chang).

Highlights

Acetate is not always an end product in acetogen metabolism.

The reaction mechanism of butyrate production with acetate uptake was identified.

Greater NADH oxidation facilitates the catabolic (carbon monoxide oxidation) reaction rate.

The metabolic shift from acetogenesis to ethanologenesis occurs via complete acetate uptake.

The shift to a single volatile product enables the yield and selectivity of target products to be enhanced.

Trends in Biotechnology, March 2025, Vol. 43, No. 3
https://doi.org/10.1016/j.tibtech.2024.11.008

Trends in Biotechnology

CellPress OPEN ACCESS

Research Article

Acetogenesis to ethanologenesis: facilitating NADH oxidation via reductive acetate uptake

Soyoung Oh [1,2,10], Jiyeong Jeong [1,10], Byeonghyeok Park [3], Byeongchan Kang [1], Ji-Yeon Kim [1,2], Sehoon Park [4], Dong-Hun Lee [5,9], Seunghyeon Jung [4], Mungyu Lee [1,2], Wonjung Lee [6], Muhammad Yasin [7], Junhyeok Seo [2,6], Zee-Yong Park [4], Kyung-Hoon Shin [5], Volker Müller [8], In-Geol Choi [3,*], and In Seop Chang [1,2,*]

(Homo)acetogens, including *Clostridium* spp., represent an enigma in metabolic flexibility and diversity. *Eubacterium callanderi* KIST612 is an acetogen that produces n-butyrate with carbon monoxide (CO) as the carbon and energy source; however, the production route is unknown. Here, we report that its distinctive butyrate formation links to reductive acetate uptake, suggesting that acetate (the end-product) is reuptake, leading to a physiological advantage through NADH oxidation. Thus, we introduced an ethanol production pathway from acetyl-CoA as a competitive pathway for butyrate production. Consequently, the metabolic pathway in our mutants switched from acetogenesis to 'ethanologenesis', eliminating butyrate production and the uptake of previously produced acetate. The metabolic shifts occurred toward greater NADH oxidation, facilitating CO oxidation and productivity, which is a survival mechanism at the thermodynamic edge. This metabolic shift to a single product holds potential to revolutionize product separation strategies in synthetic gas (syngas)-based biorefineries.

Introduction

Recent biotechnology advances highlight the potential of syngas fermentation to mitigate anthropogenic carbon emissions by converting both natural (e.g., coal and biomass) and waste (e.g., municipal solid waste) feedstock into liquid chemicals [1]. However, the production of multiple products results in separation complexities and increased operating costs. Therefore, the realization of commercial syngas fermentation lies in developing strains yielding high titers of a single product. This requires the study of specific acetogen strains to understand their metabolic pathways and optimize their product profiles.

Acetogens have remarkable metabolic flexibility, enabling them to grow autotrophically and heterotrophically and ensuring their survival in diverse ecosystems [2,3]. Acetogens fix carbon via the Wood–Ljungdahl pathway (WLP), also termed the 'reductive acetyl-CoA pathway' [4]. During the autotrophic growth of acetogens, WLP and chemiosmotic energy conservation (CEC) are coupled, indicating that reducing equivalents (e.g., NADH or ferredoxin [Fd^{2}]) are involved in ATP conservation and consumption [5]. Many acetogens primarily produce acetate, but some strains generate more reduced end products, such as ethanol, and/or C4-containing compounds, including butyrate and butanol [6,7]. However, acetate is energetically more favorable than other products [8], and the reasons for the production of these reduced chemicals, specifically during lithoautotrophic growth, remain elusive.

Eubacterium callanderi KIST612 (formerly *Eubacterium limosum* KIST612) is a Gram-positive acetogen originally isolated from an anaerobic digester [9] and recently reclassified as *Eubacterium*

Technology readiness

In acetogens, acetate production is crucial for energy conservation under autotrophic conditions. Theoretical ATP yield has been a key factor when engineering strains for butyrate, ethanol, and other products via carbon monoxide (CO) fermentation. In the present study, we proposed a strategy to overcome low ATP yields by enhancing metabolic reaction rates linked to NADH oxidation and energy conservation. We identified the butyrate production pathway and demonstrated the approach by constructing an ethanol-producing strain. Ethanol production with complete acetate uptake were validated in batch mode. The current Technology Readiness Level (TRL) is 1–3, with large-scale fermentation trials and process optimization required for industrialization. Ethanol production with acetate uptake offers enhanced metabolic reaction rates, high selectivity, and product yield, reducing operational costs and improving product recovery. Using industrial off-gas and synthetic gas (syngas) alongside CO for ethanol production could also serve as a CO_2 reduction technology.

[1]School of Environment and Energy Engineering, Gwangju Institute of Science and Technology, 123 Cheomdan-gwagiro, Buk-gu, Gwangju 61005, Republic of Korea
[2]Research Center for Innovative Energy and Carbon Optimized Synthesis for Chemicals, Gwangju Institute of Science and Technology, 123 Cheomdan-gwagiro, Buk-gu, Gwangju 61005, Republic of Korea
[3]Department of Biotechnology, College of Life Sciences and Biotechnology, Korea University, 145 Anam-ro, Seongbuk-gu, Seoul 02841, Republic of Korea

callanderi based on genome analyses [10,11]. This strain can grow with H_2/CO_2 as well as considerably high CO partial pressure (~200 kPa) without significant substrate inhibition [12]. Its metabolic features under various conditions have been well studied and reported [7,9,10,13,14]. Notably, the strain produces butyrate from CO, but the route and reason for the production of this compound are unknown [7,14].

This study used *E. callanderi* KIST612 as a model strain to elucidate the reasons behind its unique metabolic features and versatility to produce butyrate from CO. We hypothesized that butyrate production may offer physiological benefit(s), such as NADH regeneration and facilitation of a high metabolic reaction rate, even if energetically less favorable. To demonstrate this, we reprogrammed the KIST612 strain to have an ethanol production pathway that allows for more NADH oxidation and acetate uptake. These findings provide new insights into the metabolic versatility and flexibility of CO-utilizing acetogens, which could help the commercial syngas-based biorefinery sector by streamlining product outputs and optimizing energy balances.

Results

Butyrate production exhibited different metabolic patterns between glucose and CO conditions

E. callanderi KIST612 exhibited metabolic diversity by producing acetate and butyrate as end products under autotrophic H_2/CO_2 (AH), autotrophic CO (AC), and heterotrophic glucose (HG) conditions. In AH conditions, acetate was produced but not butyrate (Figure 1A). Butyrate production started during the late exponential to stationary phases in AC conditions (Figure 1B). In HG conditions, both acetate and butyrate simultaneously accumulated throughout the growth phase (Figure 1C). We initially performed transcriptome analyses of cells growing in the mid-log (ML) and early stationary (ES) phases in HG, AC, and AH conditions (Figure S1 in the supplemental information online); differentially expressed genes (DEGs) found in each growth condition are shown as reads per kilobase of transcript per million mapped reads (RPKM) values in Figure S1A,B. Based on the six groups for DEG classification, the expression patterns of genes belonging to the central carbon and energy metabolism pathways are also shown (Figure S1C). Transcripts of most glycolytic genes were upregulated in HG conditions, whereas transcripts related to gluconeogenesis were upregulated in both autotrophic conditions (Table S1 in the supplemental information online). Transcripts related to WLP genes were upregulated exclusively under AC and AH conditions. Within the methyl branch of the WLP, formate dehydrogenase (Fdh; EC 1.2.1.2; ELI_0994 and ELI_3306) and formyltetrahydrofolate synthetase (FTHFS; EC 6.3.4.3; ELI_0372) exhibited upregulation during the ES phase under AC conditions (Table S1). Transcripts of genes encoding electron bifurcating-hydrogenase, Rnf complex, and ATP synthase related to WLP and the CEC mechanism were also highly induced in cells grown in autotrophic conditions (Table S1).

Proteome analysis was performed with AC-, AH-, and HG-grown cells in the ES growth phase. The RPKM value and protein abundance are presented in Figure S2 and Tables S2 and S3 in the supplemental information online. Here, we focused on the butyrate production pathway in AC conditions. The proteins associated with energy metabolism, including the Rnf complex and ATP synthase, in addition to butyrate production-related enzymes, showed $\log_2FC \geq 1$ in both the transcriptome and proteome data sets (Figure 1D). The abundance of the protein catalyzing butyryl-CoA formation from acetyl-CoA increased in AC-grown cells was similar to that in HG-grown cells (Figure 1E). The translational level of phosphotransbutyrylase (Ptb) was upregulated in AC-grown cells, but not the transcriptional level of *ptb*. The genome of KIST612 encodes three potential CoAT genes (ELI_2854, ELI_3452, and ELI_3772), the transcriptional levels of which were higher in AC-grown cells than in HG-grown cells.

[4]School of Life Sciences, Gwangju Institute of Science and Technology, 123 Cheomdan-gwagiro, Buk-gu, Gwangju 61005, Republic of Korea
[5]Department of Marine Sciences and Convergent Technology, Hanyang University, Ansan 15588, Republic of Korea
[6]Department of Chemistry, Gwangju Institute of Science and Technology, 123 Cheomdan-gwagiro, Buk-gu, Gwangju 61005, Republic of Korea
[7]Department of Chemical Engineering, COMSATS University Islamabad, Lahore, 54000, Pakistan
[8]Molecular Microbiology & Bioenergetics, Institute of Molecular Biosciences, Johann Wolfgang Goethe University, Frankfurt am Main, 60438 Frankfurt, Germany
[9]Present address: Division of Earth and Environmental System Sciences, Pukyong National University, 45, Yongso-ro, Busan 48513, Republic of Korea
[10]These authors contributed equally to this study

*Correspondence:
igchoi@korea.ac.kr (I.-G. Choi) and
ischang@gist.ac.kr (I.S. Chang).

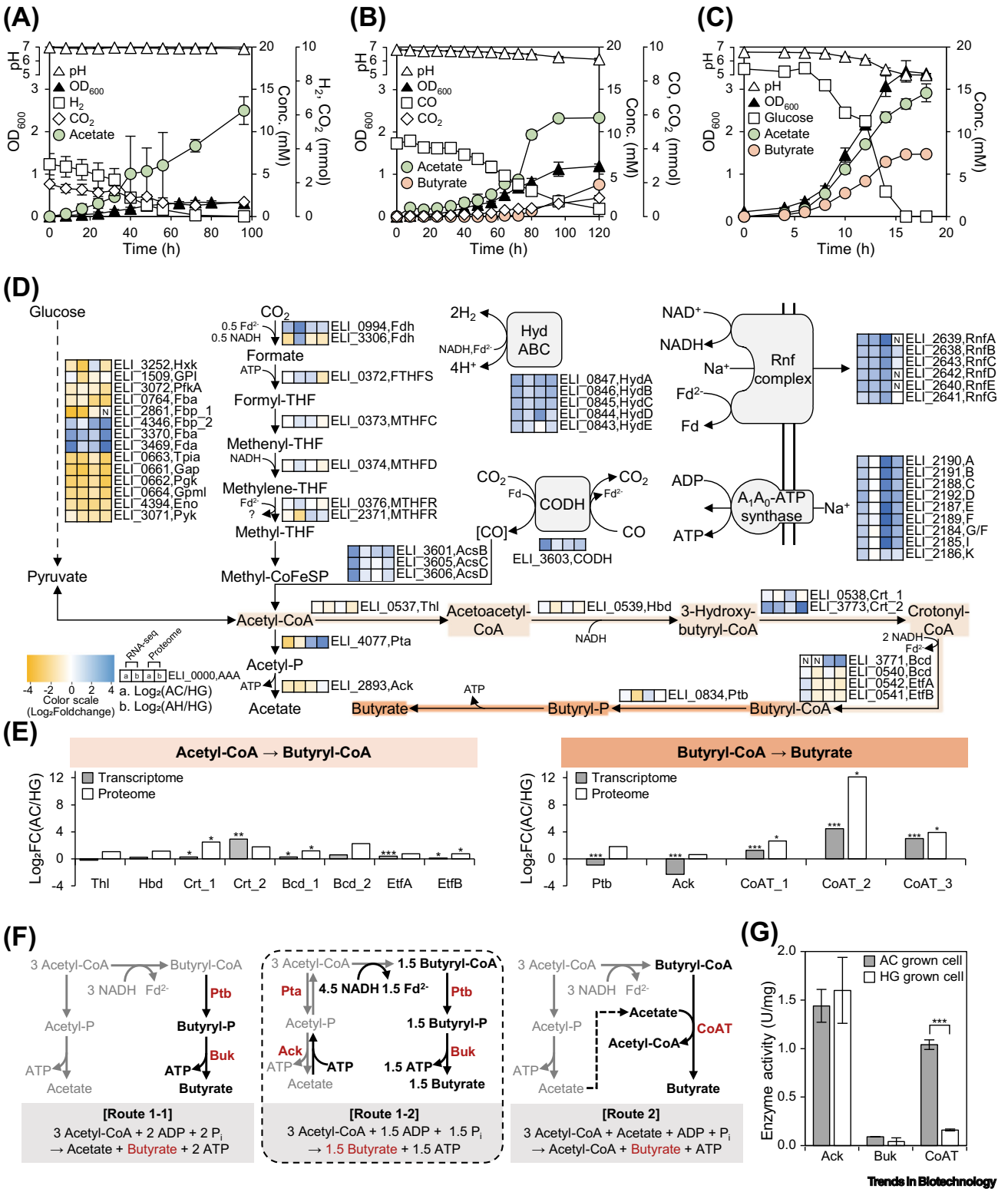

(See figure legend at the bottom of the next page.)

Growth data and 'omics analyses suggest two possible routes for butyrate formation from butyryl-CoA: Route 1-1 via Ptb and butyrate kinase (Buk), and Route 2 through butyryl-CoA: acetate CoAT (Figure 1F). In route 1-1, Ptb and consequent Buk reactions produce butyrate from butyryl-CoA via butyryl phosphate. In this route, one ATP is gained through dephosphorylation of butyryl phosphate to butyrate by Buk per two moles of acetyl-CoA for condensation. Route 2 couples with acetate uptake by CoAT, which catalyzes the transfer of the CoA moiety from butyryl-CoA to acetate. In the butyrate production pathway by CoAT reaction, ATP can be obtained only through acetate production.

The specific activities of Ack, Buk, and CoAT in both pathways were determined in cell-free extracts. Notably, the activities of Buk, although not annotated in the genome, were also detected in both AC- and HG-grown cells. The specific activity of Buk in AC-grown cells was twofold higher than that in HG-grown cells (Figure 1G). However, none of the Buk and Ack activities were statistically different between AC- and HG-grown cells. The specific CoAT activity of AC-grown cells was sixfold higher than that of HG-grown cells (P <0.001; Figure 1G). Therefore, we hypothesized that either the CoAT reaction would be dominated or the Buk reaction would be used under CO autotrophic conditions.

Butyrate production with acetate uptake is linked to NADH oxidation in CO autotrophy

To investigate whether butyrate production is linked to acetate uptake, the strain was cultivated in 30 mM sodium [1,2-$^{13}C_2$] acetate, which was exogenously supplied together with CO. During exponential growth, the [1,2-$^{13}C_2$] acetate concentration decreased, while the butyrate concentration increased proportionally (Figure 2A). During the cell growth phase, isotopic patterns showed a reverse logarithmic correlation (R^2=0.782) between acetate and butyrate. For acetate, the ^{12}C composition derived from CO as energy and carbon sources gradually started increasing during the early growth phase, whereas the composition of ^{13}C from [1,2-$^{13}C_2$] acetate decreased (Figure 2B). Conversely, for butyrate, ^{13}C-enrichment was 37% at the beginning of the growth phase and remained between 40% and 60%, reaching a peak of 63.6% (Figure 2C). This demonstrates that, as the metabolic end-product of acetogenesis, acetate can be utilized into butyrate during growth on CO.

The higher specific activities of CoAT in AC-grown cells compared with those in HG-grown cells led us to consider whether CoAT has an important role in butyrate production with acetate uptake. To identify a key enzyme for the butyrate production with acetate uptake, acetate: butyryl-CoA CoAT specific activity was measured with three purified CoATs. Two CoATs

Figure 1. Metabolic characteristics of *Eubacterium callanderi* KIST612 depending on different electron/carbon sources. *E. callanderi* KIST612 was cultured using 60 ml of HEPES-buffered basal medium (HBBM) in 158-ml serum bottles. For this, 101.3 kPa of gaseous H_2/CO_2 (80:20, v/v) or carbon monoxide (CO), or 20 mM glucose were used as the carbon and electron sources: (A) autotrophic H_2/CO_2 (AH) condition, (B) autotrophic CO (AC) condition, and (C) heterotrophic glucose (HG) condition. (D) Omics data of central metabolism. Blue and yellow colors indicate that genes/proteins were upregulated/downregulated, respectively in autotrophically grown cells compared with those in heterotrophically grown cells. (E) The genes/proteins for butyrate formation were compared with Log_2Fold change (AC/HG). (F) The pathway of butyrate formation was divided into butyryl-CoA formation from acetyl-CoA (left) and butyrate formation from butyryl-CoA (right). Pathway candidates for butyrate formation from acetyl-CoA. Route 1-1: one ATP gained via phosphotransbutyrylase (Ptb)-butyrate kinase (Buk) (left); Route 1-2: butyrate production with acetate uptake occurs through ATP hydrolysis via reverse phosphotransacetylase (Pta)-acetate kinase (Ack) (broken box, middle); Route 2: butyrate production with acetate uptake via CoA transferase (CoAT) (right). (G) Specific enzyme activities in cell-free crude extracts of *E. callanderi* KIST612. One unit (U) was defined as the amount of the enzyme that catalyzed the conversion of 1 μmol of acetate (enzyme; Ack, CoAT) or butyrate (enzyme; Buk) consumed per minute. Abbreviations: AcsB, acetyl-CoA synthase; AcsC, acetyl-CoA decarbonylase/synthase subunit gamma; AcsD, acetyl-CoA decarbonylase/synthase subunit delta; Bcd, butyryl-CoA dehydrogenase; CODH, CO dehydrogenase; Crt, crotonase; Eno, phosphopyruvate hydratase; Etf, electron transfer flavoprotein; Fba, class II fructose-1,6-bisphosphate aldolase; Fbp_1, class II fructose-bisphosphate aldolase; Fbp_2, fructose-bisphosphatase class III; Fda, class I fructose-bisphosphate aldolase; Fdh, formate dehydrogenase; FTHFS, formyl tetrahydrofolate synthase; Gap, type I glyceraldehyde-3-phosphate dehydrogenase; GPI, glucose-6-phosphate isomerase; Gpml, phosphoglycerate mutase; Hbd, hydroxybutyryl-CoA dehydrogenase; Hxk, hexokinase; Hyd, hydrogenase; MTHFC, methenyl tetrahydrofolate cyclohydrolase; MTHFD, methylene tetrahydrofolate dehydrogenase; MTHFR, methylene tetrahydrofolate reductase; N, not detected; PfkA, 6-phosphofructokinase; Pgk, phosphoglycerate kinase; Pta, phosphotransacetylase; Pyk, pyruvate kinase; Rnf, sodium ion-translocating Fd:NAD^+ oxidoreductase; Thl, thiolase; TpiA, triose-phosphate isomerase. *P <0.05; **P <0.01; ***P <0.001.

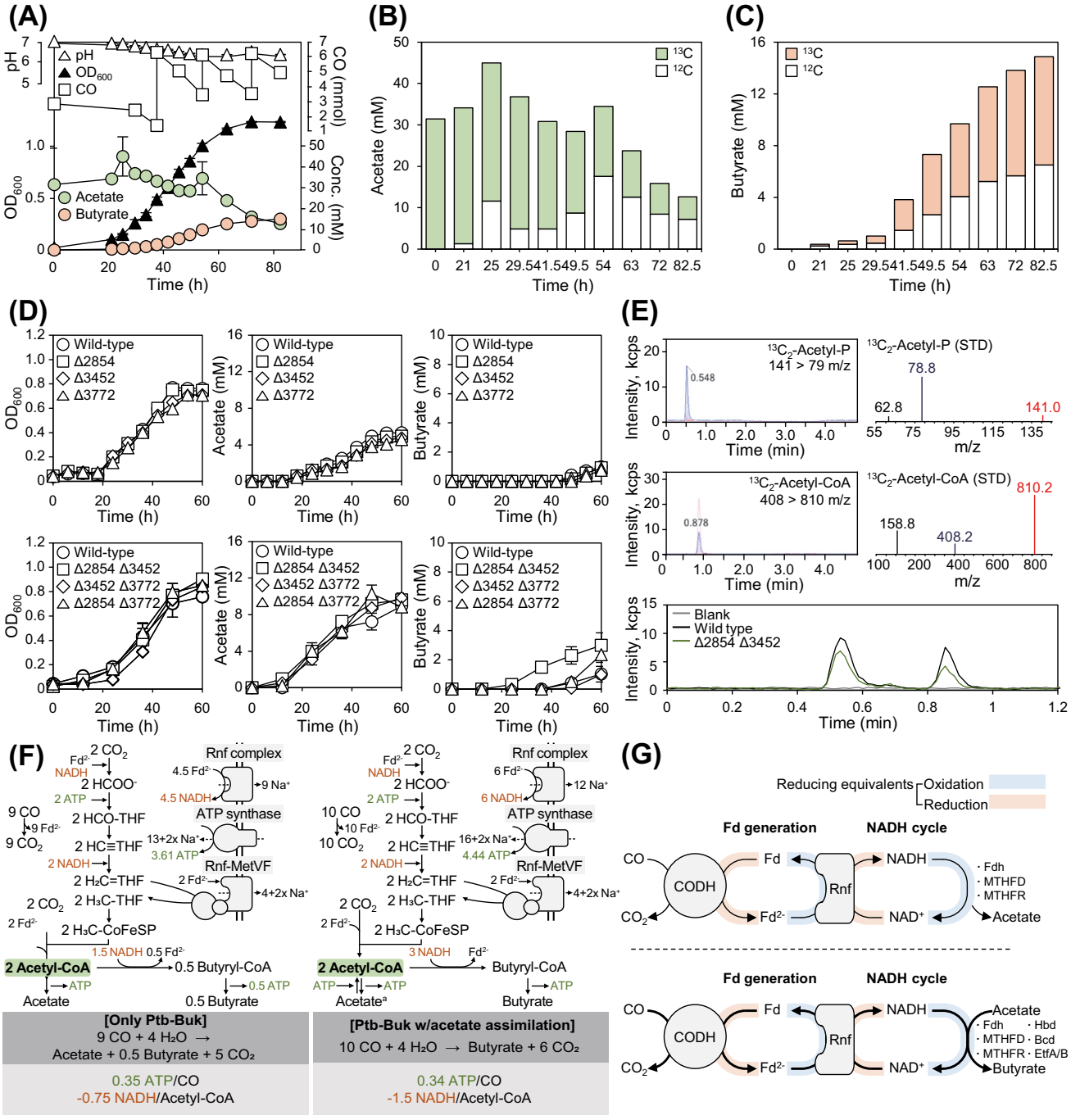

Figure 2. Butyrate production with acetate uptake in *Eubacterium callanderi* KIST612. To validate butyrate production during which acetate is utilized, *E. callanderi* KIST612 (wild-type) was cultured under carbon monoxide (CO) conditions with [1,2-$^{13}C_2$] acetate supplementation. (A) Growth and total metabolites profile, (B) isotope-labeled acetate concentration, and (C) isotope-labeled butyrate concentration. (D) Growth and product profile of single or double CoA transferase (CoAT)-deficient strains under CO growth. (E) Intracellular acetyl phosphate (acetyl-P) and acetyl-CoA detection in double CoAT-deficient strain (*E. callanderi* Δ2854 Δ3452) under CO growth. (F) Bioenergetics for butyrate production in *E. callanderi* KIST612. Butyrate is converted from butyryl-CoA via either phosphotransbutyrylase (Ptb)-butyrate kinase (Buk) (left) or Ptb-Buk with reverse phosphotransacetylase (Pta)-acetate kinase (Ack) (right). The theoretical yield of ATP/CO and NADH/acetyl-CoA was calculated. We considered the methylene tetrahydrofolate reductase (MTHFR) reaction as a sodium ion-translocating Fd:NAD$^+$ oxidoreductase (Rnf)-MetVF

(Figure legend continued at the bottom of the next page.)

(ELI_2854 and ELI_3452) exhibited activity for butyrate production with acetate conversion, while the other one (ELI_3772) did not (Figure S3A in the supplemental information online). To confirm the physiological role of CoATs in KIST612, we constructed single and double CoAT-knockout mutants (Table S5 in the supplemental information online). Although CoATs have enzyme activity for butyrate production with acetate conversion, there was no significant suppression of butyrate production on any CoAT-deficient mutants during growth on CO (Figure 2D). Notably, a double CoAT-knockout mutant (Δ2854Δ3452) showed more butyrate production compared with the wild-type.

Given that the reverse reaction of Pta-Ack with ATP hydrolysis is another pathway to achieve butyrate production with acetate uptake (see acetate uptake in route 1-2 to synthesize butyrate from butyryl-CoA in Figure 1F, broken box), we explored whether the reverse Pta-Ack occurred *in vivo*. [1,2-$^{13}C_2$] acetyl phosphate was synthesized to confirm the acetate uptake pathway (Figure S4 in the supplemental information online). We detected [1,2-$^{13}C_2$] acetyl phosphate and [1,2-$^{13}C_2$] acetyl-CoA in CO-grown cells supplemented with [1,2-$^{13}C_2$] acetate (Figure 2E). In addition, conversion of acetate to acetyl phosphate was detected with recombinant Ack protein *in vitro* (Figure S3B). Furthermore, we revealed that Ack could replace Buk through a reaction in which butyrate is converted to butyryl phosphate by Ack (Figure S3B).

This finding allows us to calculate bioenergetics using Ptb-Buk as the butyrate production pathway and reverse Pta-Ack as the acetate uptake pathway in CO metabolism of KIST612 (Figure 2F). The formation of acetate from CO occurs according to the following reaction:

$$4\ CO + 2\ H_2O \rightarrow Acetate + 2\ CO_2 + 1.39\ ATP \quad [1]$$

The formation of butyrate from CO occurs according to the following reaction (Figure S5 in the supplemental information online):

$$10\ CO + 4\ H_2O \rightarrow Butyrate + 6\ CO_2 + 3.44\ ATP \quad [2]$$

Acetate is the primary product and is essential for ATP generation in CO metabolism. In addition, the reuptake of secreted acetate is necessary for the production of butyrate as the sole end product. Here, based on two moles of acetyl-CoA, the ratio of acetate to butyrate was set at 1:0.5 to present the bioenergetics. If butyrate is generated from 2 moles of acetyl-CoA by Ptb-Buk without acetate uptake, the ATP yield per CO is 0.35. By contrast, butyrate production with acetate uptake by reverse Pta-Ack consumes 1 mole of ATP; thus, the ATP yield per CO is 0.34. Since acetate is consumed to produce butyrate, twice as much butyrate can be produced. The butyrate production with acetate uptake reaction facilitates NADH oxidation twice as much compared with that in the absence of acetate uptake (–1.5 versus –0.75 NADH/acetyl-CoA). NADH oxidation is linked to energy conservation mechanisms, such as Rnf and ATP synthase, when CO is used as an electron donor (Figure 2G). Thus, butyrate production with acetate uptake, through ATP investment, offers an advantage by reducing equivalent disposal.

Ethanologenesis with acetate uptake is reprogrammed as a newly NADH oxidation pathway

According to our hypothesis, CO metabolism would select a pathway that consumes more NADH through acetate uptake. We introduced an ethanol production pathway that competes with butyrate production and NADH oxidation, with acetyl-CoA as the branch point. We

complex reaction (Table S4 in the supplemental information online). [a]Acetate is first produced and then used as a carbon source. (G) Scheme of metabolic energy cycle with NADH oxidation in acetogen. The oxidation of NADH is linked to chemiosmotic energy conservation (CEC) mechanisms (upward). Acetate uptake can contribute to facilitate the metabolic energy cycle and product formation with NADH oxidation (downward).

proposed three potential pathways for producing ethanol from acetyl-CoA and implemented a pathway (Route 3) (Figure 3A–C). The potential pathways included: (1) WLP-mediated acetyl-CoA synthesis from CO_2 and reduction to ethanol via two NADH-consuming reduction steps by either bifunctional aldehyde/alcohol dehydrogenase (AdhE) or aldehyde dehydrogenase (Aldh)-alcohol dehydrogenase (Adh); (2) acetate reduction to aldehyde by aldehyde:ferredoxin oxidoreductase (AOR) with Adh; and (3) ethanol production with acetate uptake pathway using reverse Pta-Ack and acetyl-CoA to ethanol via two NADH consuming reduction steps. Pathway 1, in which 2 moles of acetyl-CoA are produced from 4 moles of CO_2, and each is consequently converted to 1 mole of acetate and ethanol, respectively, is a 'direct' ethanol-production pathway

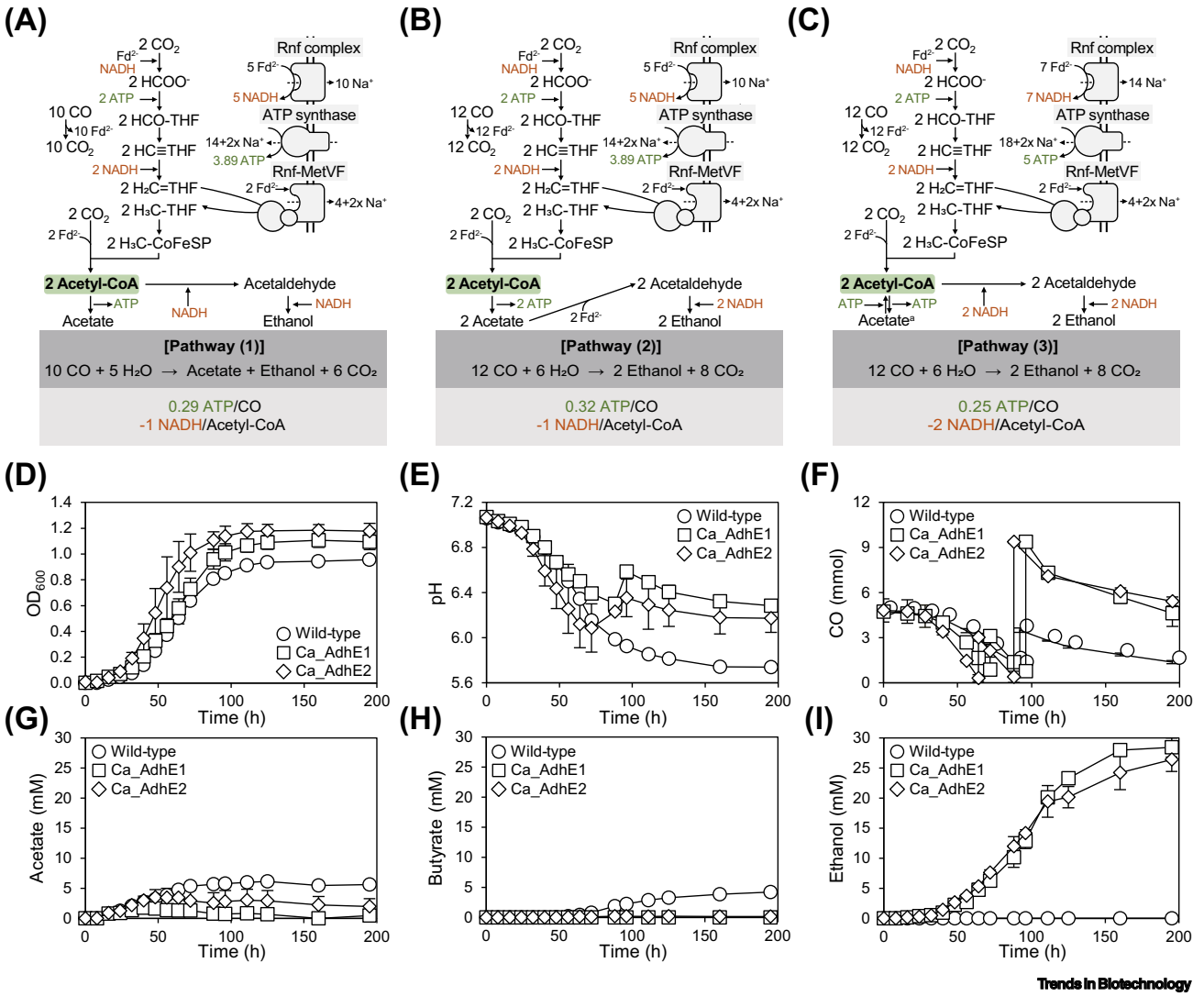

Figure 3. Ethanol production with acetate uptake in *Eubacterium callanderi* KIST612. Bioenergetics of different ethanol production pathways: (A) direct ethanol production pathway via either aldehyde dehydrogenase (Aldh)-alcohol dehydrogenase (Adh) or bifunctional aldehyde/alcohol dehydrogenase (AdhE). (B) Ethanol production with acetate uptake via acetaldehyde:Fd oxidoreductase (AOR)-Adh. (C) Ethanol production with acetate uptake via reverse phosphotransacetylase (Pta)-acetate kinase (Ack) and either Aldh-Adh or AdhE. [a]Acetate is first produced and then used as a carbon source. Culture profile of Ca_AdhE1, Ca_AdhE2, and *E. callanderi* KIST612 (wild-type) (D–I). All strains were cultured using 60 ml of HBBM in 158-ml serum bottles using carbon monoxide (CO) as the substrate. CO was supplemented until it was no longer consumed. (D) Optical density, (E) pH, (F) CO (mmol of gaseous CO in headspace of serum bottle), (G) acetate concentration, (H) butyrate concentration, and (I) ethanol concentration.

(Figure 3A). In Pathway 2, 2 moles of acetate are produced from 2 moles of acetyl-CoA and subsequently reduced to ethanol by alcohol dehydrogenase, mediated by reduced Fd-dependent AOR (Figure 3B). It was previously reported that *E. callanderi* KIST612 can produce ethanol, even though ethanol production was <1 mM under CO autotrophy and acetate supplementation [13]. In Pathway 3, 1 mole of acetate produced in the direct pathway of acetogenesis is converted into acetyl-CoA through the reverse Pta-Ack pathway and then reduced to ethanol through the Aldh-Adh reaction (Figure 3C). When comparing ATP/CO yield, Pathways 1 and 2 are the most energetically favorable, providing 0.29 and 0.32 ATP/CO, respectively. Ethanol production with acetate uptake via the reverse reaction of Pta-Ack is more advantageous in terms of NAD(H) regeneration, even if it does not offer the same ATP yield per mol of CO. This reverse pathway of Pta-Ack oxidizes twice as much NADH compared with AOR-mediated aldehyde reduction to ethanol.

To construct the new metabolic pathway that can consume more NADH than the butyrate production pathway, *adhE1* (CAETHG_3747) or *adhE2* (CAETHG_3748) of *Clostridium autoethanogenum* DSM 10061 (an ethanol-producing strain) were heterologously expressed in *E. callanderi* KIST612. Two transformants (Ca_AdhE1 and Ca_AdhE2) showed different metabolism and product formation compared with the wild-type. The optical density of both AdhE transformants was also higher than that of the wild-type (Figure 3D). The growth rates of the strains were as follows: 0.08±0.01 h^{-1} in KIST612, 0.07±0.01 h^{-1} in Ca_AdhE1, and 0.07±0.01 h^{-1} in Ca_AdhE2. The pH was subsequently increased with extracellular acetate reuptake in the exponential phase (Figure 3E). Both transformants consumed 11.5 moles of CO, which was almost twofold higher than that observed in the wild-type (Figure 3F). Both Ca_AdhE1 and Ca_AdhE2 cultures showed acetate production during the exponential phase, with subsequent decreases, possibly in favor of ethanol production (Figure 3G). Ca_AdhE1 and Ca_AdhE2 mainly produced 1.31 g l^{-1} and 1.22 g l^{-1} of ethanol, respectively, while the wild-type produced butyrate (Figure 3H,I), indicating that the pathways of these two metabolites (butyrate and ethanol) were competing at the acetyl-CoA branching point. All culture parameters and data analyzed for the three cultures are shown in Table 1.

In the state of decreasing acetate concentration, assuming conditions of acetate uptake, AdhE mutants exhibited greater CO consumption rates (more than tenfold) and acetate production rates (more than fourfold) compared with wild-type. Ethanol production promotes NAD^+

Table 1. Kinetic parameters and intracellular redox state in Ca_AdhE1, Ca_AdhE2, and *Eubacterium callanderi* KIST612[a,b]

	Kinetic parameters (mmol l^{-1} h^{-1} $gCDW^{-1}$)								Intracellular redox state
	CO consumption rate[c]		Acetate production rate[d]		Butyrate production rate[d]		Ethanol production rate[d]		
State of acetate concentration	IN[e]	DE[f]	IN	DE	IN	DE	IN	DE	[NADH]/[NAD^+]
E. callanderi KIST612	0.15±0.03	0.06±0.01	0.43±0.01	-0.03±0.04	0.23±0.00	0.05±0.01	–[g]	–	0.05±0.01
Ca_AdhE1	2.30±1.12	0.80±0.01	1.77±0.20	-0.12±0.08	–	–	1.06±0.06	1.35±0.02	0.27±0.12
Ca_AdhE2	3.98±1.40	0.40±0.07	2.05±0.11	-0.01±0.03	–	0.03±0.05	1.26±0.17	0.89±0.28	0.14±0.13

[a]Based on the maximum acetate concentration, each kinetic parameter was calculated during the period of increasing (IN) and decreasing (DE) acetate concentration.
[b]Data are mean ± standard deviation. The standard deviation was obtained from duplicate samples, other than for the intracellular redox state, where it was obtained among three independently repeated experiments.
[c]CO consumption rates were determined for the following growth sampling times: 16–111 h for IN and 125–195 h for DE in the KIST612 strain; 0–28 h and 40–72 h for IN and DE, respectively, in Ca_AdhE1; 0–28 h and 64.1–88 h for IN and DE, respectively, in Ca_AdhE2.
[d]For product production rate, the IN and DE of *E. callanderi* KIST612 were 16–111 h and 125–160 h, and the IN and DE of Ca_AdhE1 were 16–32 h and 40–72 h, respectively. The IN and DE of Ca_AdhE2 were 16–40 h and 48–64 h, respectively.
[e]At increase of acetate concentration.
[f]At decrease of acetate concentration.
[g]Not detected.

regeneration, and the increase in CO consumption rate may be coupled with Rnf to regenerate NADH, thereby potentially influencing the NADH/NAD^+ ratio. The NADH/NAD^+ ratio in KIST612 was further decreased to 0.05 compared with 0.1 in *C. autoethanogenum* in CO-grown cells [15]. However, the NADH/NAD^+ ratio of Ca_AdhE1 and Ca_AdhE2 was higher (0.27±0.12 and 0.14±0.13), demonstrating a more reduced state in these strains (Table 1). We argue that NAD^+ regeneration via ethanol production contributes to increasing the overall metabolic energy cycle, including CO oxidation. Notably, extracellular acetate was completely taken up during the stationary phase in Ca_AdhE1 but not in Ca_AdhE2. The degree of acetate reduction was reflected by differences in enzyme activities of AdhE. Ca_AdhE1 exhibited the highest acetaldehyde dehydrogenase activity (Table S6 in the supplemental information online). Moreover, there was no significant difference in enzyme activity of Adh between the two transformants and wild-type (P=0.07).

We validated ethanol production with acetate uptake via ^{13}C enrichment analysis using Ca_AdhE1 in CO autotrophy (Figure 4A). We determined 64% $^{13}C_2$-ethanol enrichment with 31 mM [1,2-$^{13}C_2$] acetate consumption (Figure 4B,C). The ^{13}C-labeled butyrate was enriched by up to 7% (Figure 4C). The kinetics of acetate consumption and ethanol production were calculated during the time period 72–82.5 h, in which the $^{12}C_2$-acetate concentration decreased

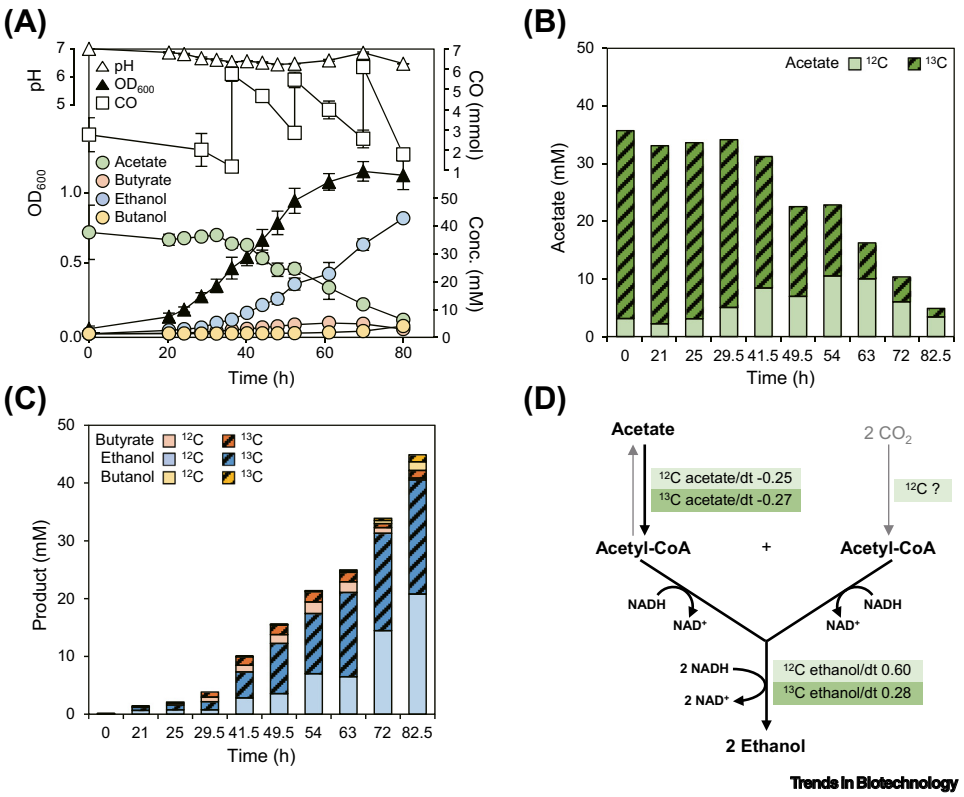

Figure 4. ^{13}C enrichment analysis of Ca_AdhE1 under carbon monoxide (CO) conditions. Ca_AdhE1 was cultured using 80 ml of HBBM in 158-ml serum bottles. (A) Profile of growth and total metabolites. CO (mmol) was measured in the headspace gas of the serum bottle, (B) concentration of acetate, (C) concentration of butyrate, ethanol, and butanol, and (D) kinetic analysis of acetate consumption and ethanol production in the 72–82.5 h period, in which $^{12}C_2$ acetate concentration decreased. Acetate consumption rate (mmol l^{-1} h^{-1}) and ethanol production rate (mmol l^{-1} h^{-1}) were calculated for both ^{12}C and ^{13}C.

(Figure 4D). The ethanol/acetate yield, calculated based on the combined amounts of unlabeled and ^{13}C-labeled products, was 1.69. The $^{13}C_2$-ethanol/$^{13}C_2$-acetate yield was 1.02 when the $^{13}C_2$-acetate consumption rate was 0.27 mmol l^{-1} h^{-1} and the $^{13}C_2$-ethanol production rate was 0.28 mmol l^{-1} h^{-1}. The $^{12}C_2$-ethanol/$^{12}C_2$-acetate yield was 2.62 when the $^{12}C_2$-acetate consumption rate was 0.25 mmol l^{-1} h^{-1} and the $^{12}C_2$-ethanol production rate was 0.60 mmol l^{-1} h^{-1}. The fact that the ethanol production rate was twice as high as that of acetate reuptake means that ethanol is produced from CO in addition to acetate reuptake.

In addition, the highest CO consumption rate was monitored during the 72–82.5 h period, suggesting that ethanol production with acetate uptake promotes CO oxidation kinetics, and conclusively facilitates the entire metabolic cycle, such as the Rnf complex and the ATP synthase from Fd^{2-} derived from CO oxidation. In addition, the detection of $^{13}C_2$-acetyl phosphate in Ca_AdhE1 demonstrates that ethanol production with acetate uptake occurs via the reverse Pta-Ack reaction with ATP hydrolysis, similar to butyrate production with acetate uptake. During the [1,2-$^{13}C_2$]-acetate-consuming growth phase, 7.4±3.8 ng mgCDW^{-1} and 9.5±0.5 ng mgCDW^{-1} of $^{13}C_2$-acetyl phosphate were detected in wild-type and Ca_AdhE1, respectively (Table S7 in the supplemental information online). Conversely, in *C. autoethanogenum* DSM 10061, which utilizes AORs as an acetate conversion pathway, $^{13}C_2$-acetyl phosphate was detected at 1.2±0.1 ng mgCDW^{-1}, which was 6.2-fold lower than that of the wild-type.

Through transcriptomic and proteomic analyses, we confirmed metabolic flux generation in the ethanol production pathway in Ca_AdhE1 (Figure 5). The AdhE1-encoding gene (CAETHG_3747) was highly expressed in both omics data from strain Ca_AdhE1. Butyrate metabolism was downregulated in Ca_AdhE1 compared with that in the wild-type. Transcripts and proteins that convert acetoacetyl-CoA to butyryl-CoA (Hbd, hydroxybutyryl-CoA; EtfA/B, electron transfer flavoprotein subunit A/B; and Bcd, butyryl-CoA dehydrogenase) were significantly downregulated ($P \leq 0.05$). The KIST612 strain has three putative AOR-encoding genes (ELI_0332, ELI_1752, and ELI_3389), which convert acetate to acetaldehyde, whereas *C. autoethanogenum* has two AORs [16,17].

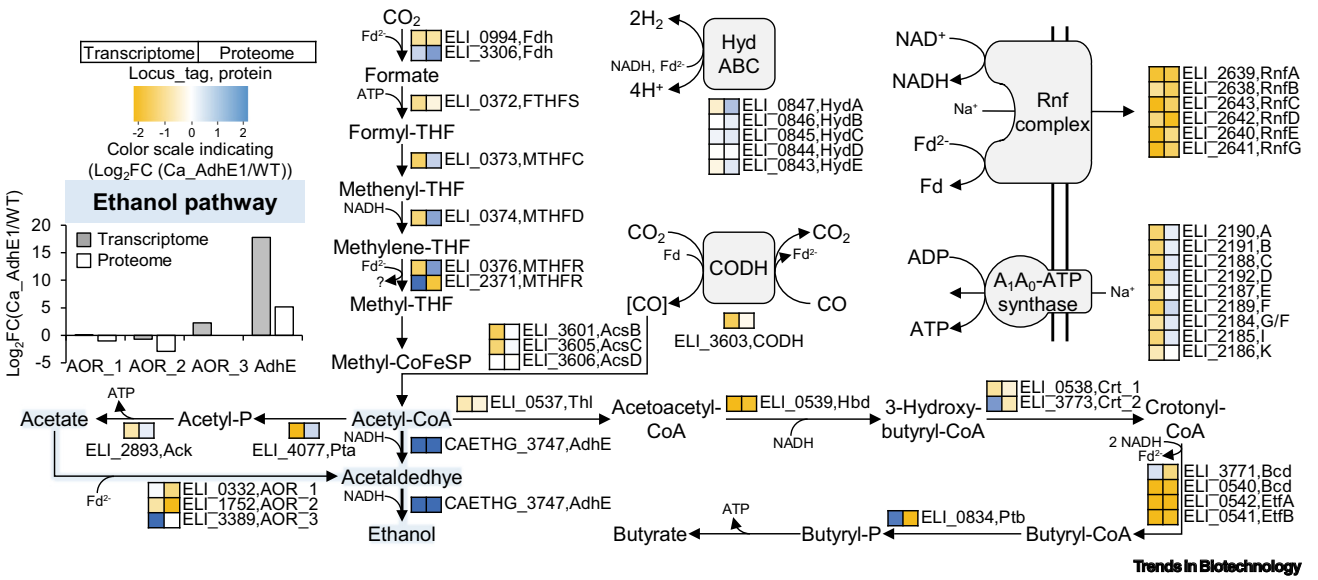

Figure 5. Differential expression level of Ca_AdhE1 compared with that of wild-type under carbon monoxide (CO) conditions. The genes/proteins related to butyrate and ethanol production were compared with Log_2Fold change (Ca_AdhE1/wild-type). Abbreviations: AdhE1, bifunctional aldehyde/alcohol dehydrogenase (CAETHG_3747); AOR, aldehyde: Fd oxidoreductase. Enzyme abbreviations are given in full in Figure 1 in the main text.

ELI_1752 is 52% identical to the AOR of *C. autoethanogenum*. ELI_1752 and ELI_0332 showed no significant change in their transcription level but were downregulated in proteome data. The FC of mRNA increased fourfold in ELI_3389 but the protein was not detected in the proteome data. Moreover, the transcription abundance of all three AORs was very low based on comparisons of RPKM values with genes involved in central metabolism. In addition, the KIST612 strain displayed 100-fold lower AOR activity compared with *C. autoethanogenum* DSM 10061 (Table S6).

Discussion

Since its isolation during the early 1990s, KIST612 has undergone extensive experimental testing to assess its physiological and metabolic features under various growth conditions, particularly in CO autotrophy [7,10,14,18–20]. This metabolic versatility is evident from the electron source-dependent butyrate production during KIST612 growth. While butyrate production in glucose heterotrophy is associated with acetate production, similar to butyrate-acetate fermentation in Clostridia [21], this is not the case in CO autotrophy.

Here, butyrate production with acetate uptake was observed and investigated during CO autotrophy, and the butyrate production pathway was identified as the Ack-driven Buk reaction. Furthermore, we revealed that the acetate uptake pathway occurs through the reverse Pta-Ack reaction, as demonstrated by the detection of $^{13}C_2$-acetyl phosphate and physiological features of CoAT mutant strains. Although the butyrate production with acetate conversion by CoATs *in vitro* was evident, these functions may contribute, in opposing directions, to the formation of other fatty acids *in vivo*, as reported in other strains with CoA transferases [22]. Butyrate production with acetate uptake requires ATP investment. Although the ATP yield is less favorable in butyrate production with acetate uptake, ATP hydrolysis leads to more NADH oxidation. In energy conservation mechanisms in autotrophic, Rnf-containing acetogens, NADH is considered a waste product that must be reoxidized by the NADH-consuming pathway [8,23]. NAD(H) oxidation or regeneration helps to synthesize ATP for energy conservation using the CEC mechanism (Figure 2G). In addition, CEC mechanisms are coupled to CO oxidation by CO dehydrogenase to generate ferredoxin and the NADH cycle in CO autotrophy. NADH oxidation with acetate uptake enhances the CO oxidation rate and productivity. These findings led us to consider that reductive acetate uptake acts in a physiological direction of greater NADH oxidation in CO autotrophy.

The engineered ethanol-producing strains demonstrated that KIST612 selects a metabolic pathway that further oxidizes NADH in CO autotrophy. The heterologous expression of NADH-dependent AdhE(s) primarily induced ethanol production rather than butyrate production. Both Ca_AdhE1 and Ca_AdhE2 promoted the central metabolic reaction rate, including acetate uptake rate (generally by more than fourfold) and CO consumption rate (generally by more than tenfold). Therefore, the ATP yield per CO in butyrate production with acetate uptake was greater than that in ethanol production with acetate uptake, but the metabolic rate was faster in ethanol production with acetate uptake. In other words, the ATP yield by bioenergetics can be overcome by physiological kinetics, such as respiratory rate, enzyme reaction rate, and metabolic reaction rate. In particular, Ca_AdhE1 showed the highest enzymatic activities of both Aldh and Adh, predominately resulting in ethanol production with complete acetate uptake driven by ATP hydrolysis. According to specific activities in *in vitro* assays, Adh should be considered as a rate-determining step; however, the difference in the degree of acetate uptake and ethanol production could be determined by Aldh activity, because acetaldehydes are likely to be rapidly converted to intermediates *in vivo*. Ethanol production with acetate uptake occurred via the reverse Pta-Ack reaction and AdhE, as evidenced by the detection of isotopically labeled acetyl phosphate. *Clostridium* spp. such as *Clostridium ljungdahlii* and *C. autoethanogenum*, have been reported to have energetically

favorable AOR reactions for ethanol production [16,24]. Although the strain KIST612 has AORs, its levels of enzymatic activity and expression are relatively low compared with those of *C. autoethanogenum* DSM 10061. Acetate uptake has been considered to maintain intracellular pH and shift the acidogenic phase to a solventogenic phase. Here, we validated that the consumption of reducing equivalents via acetate uptake drives the entire metabolic reaction rate and we assume that the metabolic versatility of the substrate may be related to this mechanism.

Since presenting bioenergetics by calculating theoretical ATP yield is a thermodynamic issue, it is conventionally considered to always take precedence over any condition or environmental change. The metabolite shifting identified in this study closely resembles the metabolic shifts seen during the acidogenic and solventogenic phases of Clostridia in acetone–butanol–ethanol fermentation. Despite extensive research on biphasic reactions in Clostridia, the science behind the causes and control mechanisms for these shifts remains unclear. Contrary to the conventional understanding that recognizes acetate as the final metabolite of acetogenesis, our findings suggest that this is not always the case. In addition, uptake of acetic acid as an end product of acetogens and converting it into a high degree of reducing substances implies that a reaction occurs in the form of ethanol production with acetate uptake. Moreover, the downregulation of genes/proteins associated with butyrate production suggests potential regulation of the redox state between the acetate production pathway and the NADH-oxidizing pathway in fermentation; thus, butyrate or ethanol could be produced as the sole end product, following a comprehensive understanding of the regulation mechanism.

Concluding remarks

Biocatalyst-based ethanol production is a more efficient approach compared with conventional high-temperature, high-pressure processes, because it reduces energy consumption. Ethanol production via an acetate uptake pathway could increase economic value by converting syngas into ethanol, a substance with a higher market value than that of acetic acid, implying a 'valorization' effect. In addition, the engineered strain for ethanol production with acetate uptake offers economic advantages by maintaining pH, improving product selectivity, and accelerating the metabolic reaction rate, potentially reducing operating costs and simplifying downstream processing in syngas fermentation. Distillation-based separation and recovery of alcohols compared with the recovery of dissociative organic acids, such as acetic acid or butyric acid, would help increase the economic efficiency of the process [25,26], and eventually improve the economic feasibility of large-scale syngas fermenting systems. Moreover, a metabolic understanding of acetate uptake could be used as a strategy to improve product yield and selectivity in the production of carbon elongation compounds, such as butyrate, butanol, and hexanoate (see Outstanding questions). This research has important implications for developing strains suitable for commercial syngas fermentation.

STAR★METHODS

Detailed methods are provided in the online version of this paper and include the following:

- KEY RESOURCES TABLE
- EXPERIMENTAL MODEL AND STUDY PARTICIPANT DETAILS
- METHOD DETAILS
  - Bacterial growth and culture conditions
  - Plasmid and strain construction
  - Enzyme assay
  - OMICS analyses
  - Instrumental analyses
- QUANTIFICATION AND STATISTICAL ANALYSIS

Outstanding questions

What are the regulatory mechanisms of the balance between butyrate and ethanol production, and how can butyrate production with complete acetate uptake be achieved?

What technical challenges are encountered in ethanologenesis in large-scale fermentation?

What factors drive both acetate production and its subsequent reuptake?

Can both the forward and reverse Pta-Ack reactions occur within a single bacterial cell?

If *AdhE* is integrated into the chromosome for antibiotic-free systems, how does this impact ethanol production?

RESOURCE AVAILABILITY

Lead contact

Further information and requests for resources and reagents should be directed to, and will be fulfilled by, the lead contact, In Seop Chang (ischang@gist.ac.kr).

Materials availability

This study did not generate new unique reagents.

Data and code availability

The transcriptome data have been deposited in the NCBI GEO database under accession number GSE149269. The mass spectrometry proteomics data have been deposited to the ProteomeXchange Consortium (http://proteomecentral.proteomexchange.org) via the PRIDE partner repository with the data set identifier PXD019256.

Any additional information required to reanalyze the data reported in this paper is available from the lead contact upon request.

Author contributions

Conceptualization, S.O., J.J., I-G.C., and I.S.C.; methodology, S.O., J.J., B.K., and J-Y. K.; formal analysis and investigation, S.O., J.J., B.K., J-Y. K., B.P., S.P., S.J., D-H.L., M.L., and W.L.; resources, V.M., Z-Y.P., J.S., K-H.S., I-G.C., and I.S.C.; writing-original draft, S.O., J.J., and I.S.C.; writing-review & editing, all authors; visualization, S.O., J.J., B.K., and B.P.; supervision, I-G.C., and I.S.C.; project administration, S.O., J.J., I-G.C., and I.S.C.; funding acquisition, I.S.C.

Acknowledgments

This work was supported by National Research Foundation of Korea (NRF) grants funded by the Korean Government (NRF-2015M3D3A1A01064883, NRF-2020R1A2C3009210, and NRF-2021R1A5A1028138) and a New & Renewable Energy Core Technology Program of the Korea Institute of Energy Technology Evaluation and Planning (KETEP) grant (No. 20173010092460) from the Ministry of Trade, Industry and Energy. We are grateful to Mostafa S. Elshahed and Michael J. Sadowsky for their assistance in reviewing and revising the paper.

Declaration of interests

J.J., B.P., I-G.C., and I.S.C. have registered patents related to this work (Patent No. KR1020733080000 and No. US11976314). All other authors declare no conflicts of interests.

Supplemental information

Supplemental information to this article can be found online at https://doi.org/10.1016/j.tibtech.2024.11.008.

References

1. Stasiek, J.A. *et al.* (2021) Gasification of densified biomass (DB) and municipal solid wastes (MSW) using HTA/SG technology. *Processes* 9, 2178
2. Fontaine, F. *et al.* (1942) A new type of glucose fermentation by *Clostridium thermoaceticum*. *J. Bacteriol.* 43, 701–715
3. Kerby, R. and Zeikus, J. (1983) Growth of *Clostridium thermoaceticum* on H_2/CO_2 or CO as energy source. *Curr. Microbiol.* 8, 27–30
4. Wood, H.G. *et al.* (1986) The acetyl-CoA pathway of autotrophic growth. *FEMS Microbiol. Rev.* 2, 345–362
5. Schuchmann, K. and Müller, V. (2014) Autotrophy at the thermodynamic limit of life: a model for energy conservation in acetogenic bacteria. *Nat. Rev. Microbiol.* 12, 809–821
6. Lanzillo, F. *et al.* (2024) Continuous HBE fermentation by *Clostridium carboxidivorans*: CO vs syngas. *New Biotechnol.* 81, 1–9
7. Litty, D. and Müller, V. (2021) Butyrate production in the acetogen *Eubacterium limosum* is dependent on the carbon and energy source. *Microb. Biotechnol.* 14, 2686–2692
8. Katsyv, A. and Müller, V. (2020) Overcoming energetic barriers in acetogenic C1 conversion. *Front. Bioeng. Biotechnol.* 8, 621166
9. Chang, I.-S. *et al.* (1997) Isolation and identification of carbon monoxide utilizing anaerobe, *Eubacterium limosum* KIST612. *Microbiol. Biotechnol. Lett.* 25, 1–8
10. Roh, H. *et al.* (2011) Complete genome sequence of a carbon monoxide-utilizing acetogen, *Eubacterium limosum* KIST612. *J. Bacteriol.* 193, 307–308
11. Kim, J.-Y. *et al.* (2023) Genome-based reclassification of strain KIST612, previously classified as *Eubacterium limosum*, into a new strain of *Eubacterium callanderi*. *J. Microbiol. Biotechnol.* 33, 1084–1090
12. Chang, I.-S. *et al.* (1998) CO fermentation of *Eubacterium limosum* KIST612. *J. Microbiol. Biotechnol.* 8, 134–140
13. Chang, I.-S. *et al.* (1999) Formulation of defined media for carbon monoxide fermentation by *Eubacterium limosum* KIST612 and the growth characteristics of the bacterium. *J. Biosci. Bioeng.* 88, 682–685
14. Park, S. *et al.* (2017) Acetate-assisted increase of butyrate production by *Eubacterium limosum* KIST612 during carbon monoxide fermentation. *Bioresour. Technol.* 245, 560–566

15. Valgepea, K. *et al.* (2018) H_2 drives metabolic rearrangements in gas-fermenting *Clostridium autoethanogenum*. *Biotechnol. Biofuels* 11, 1–15
16. Mock, J. *et al.* (2015) Energy conservation associated with ethanol formation from H_2 and CO_2 in *Clostridium autoethanogenum* involving electron bifurcation. *J. Bacteriol.* 197, 2965–2980
17. Liew, F. *et al.* (2017) Metabolic engineering of *Clostridium autoethanogenum* for selective alcohol production. *Metab. Eng.* 40, 104–114
18. Jeong, J. *et al.* (2015) Energy conservation model based on genomic and experimental analyses of a carbon monoxide-utilizing, butyrate-forming acetogen, *Eubacterium limosum* KIST612. *Appl. Environ. Microbiol.* 81, 4782–4790
19. Dietrich, H.M. *et al.* (2021) Biochemistry of methanol-dependent acetogenesis in *Eubacterium callanderi* KIST612. *Environ. Microbiol.* 23, 4505–4517
20. Kim, J.-Y. *et al.* (2021) Methanol supply speeds up synthesis gas fermentation by methylotrophic-acetogenic bacterium, *Eubacterium limosum* KIST612. *Bioresour. Technol.* 321, 124521
21. Fu, H. *et al.* (2021) Effects of benzyl viologen on increasing NADH availability, acetate assimilation, and butyric acid production by *Clostridium tyrobutyricum*. *Biotechnol. Bioeng.* 118, 770–783
22. Park, H. *et al.* (2020) Efficient, simple production of corresponding alcohols from supplemented C2-C8 carboxylic acids in *Escherichia coli* using acyl-CoA transferase from *Megasphaera hexanoica*. *Biotechnol. Bioprocess Eng.* 25, 599–606
23. Kremp, F. *et al.* (2022) A third way of energy conservation in acetogenic bacteria. *Microbiol. Spectr.* 10, e01385-22
24. Richter, H. *et al.* (2016) Ethanol production in syngas-fermenting *Clostridium ljungdahlii* is controlled by thermodynamics rather than by enzyme expression. *Energy Environ. Sci.* 9, 2392–2399
25. Fasahati, P. and Liu, J.J. (2015) Impact of volatile fatty acid recovery on economics of ethanol production from brown algae via mixed alcohol synthesis. *Chem. Eng. Res. Des.* 98, 107–122
26. Woo, H.C. and Kim, Y.H. (2019) Eco-efficient recovery of bio-based volatile C2–6 fatty acids. *Biotechnol. Biofuels* 12, 1–11
27. Jeong, J. *et al.* (2020) Genetic engineering system for syngas-utilizing acetogen, *Eubacterium limosum* KIST612. *Bioresour. Technol. Rep.* 11, 100452
28. Kang, B. *et al.* (2023) Regulatory transcription factor (CooA)-driven carbon monoxide partial pressure sensing whole-cell biosensor. *Heliyon* 9, e17391
29. Bradford, M.M. (1976) A rapid and sensitive method for the quantitation of microgram quantities of protein utilizing the principle of protein-dye binding. *Anal. Biochem.* 72, 248–254
30. Andersch, W. *et al.* (1983) Level of enzymes involved in acetate, butyrate, acetone and butanol formation by *Clostridium acetobutylicum*. *Eur. J. Appl. Microbiol. Biotechnol.* 18, 327–332
31. Scherf, U. and Buckel, W. (1991) Purification and properties of 4-hydroxybutyrate coenzyme A transferase from *Clostridium aminobutyricum*. *Appl. Environ. Microbiol.* 57, 2699–2702
32. Aceti, D.J. and Ferry, J.G. (1988) Purification and characterization of acetate kinase from acetate-grown *Methanosarcina thermophila*. Evidence for regulation of synthesis. *J. Biol. Chem.* 263, 15444–15448
33. Rauh, D. *et al.* (2004) Tungsten-containing aldehyde oxidoreductase of *Eubacterium acidaminophilum*: Isolation, characterization and molecular analysis. *Eur. J. Biochem.* 271, 212–219
34. Schönheit, P. *et al.* (1978) A rapid procedure for the purification of ferredoxin from Clostridia using polyethyleneimine. *FEBS Lett.* 89, 219–222
35. Crans, D.C. and Whitesides, G.M. (1983) A convenient synthesis of disodium acetyl phosphate for use in in situ ATP cofactor regeneration. *J. Org. Chem.* 48, 3130–3132
36. Tasnádi, G. *et al.* (2018) Evaluation of natural and synthetic phosphate donors for the improved enzymatic synthesis of phosphate monoesters. *Adv. Synth. Catal.* 360, 2394–2401

STAR★METHODS

KEY RESOURCES TABLE

Reagent or resource	Source	Identifier
Isotope labeled reagents		
Acetic acid-$^{13}C_2$	SIGMA	427039
Sodium acetate-$^{13}C_2$	SIGMA	282014
Acetyl-1,2-$^{13}C_2$ coenzyme A lithium salt	SIGMA	658650
Acetyl phosphate-$^{13}C_2$	This study	N/A
Deposited data		
Eubacterium callanderi KIST612 genome sequence	NCBI	CP002273
RNA sequencing data	This study	GEO: GSE149269
Proteomic data	This study	PRIDE: PXD019256
Other		
UV-Vis spectrophotometer	Jasco	V-730
pH meter	Metrohm	780 pH meter
Aminex HPX-87H column	Bio-Rad	1250140
GC with TCD or FID	Younglin	ACME6100 GC, ACME6000 GC
Carboxen1000 column	Supelco	60/80 Carboxen1000 column
HayeSep D column	Hayes Separation	100/120 HayeSep D column
Capillary column	Alltech	AquaWax
Hewlett-Packard 7890N series GC	Agilent	N/A
LC-40	Shimadzu	www.ssi.shimadzu.com/products/liquid-chromatography/hplcuhplc/nexera-series/index.html
AB SCIEX 4500 Q-Trap	Sciex	https://sciex.com/products/mass-spectrometers/qtrap-systems/qtrap-4500-system
Gemini C18 column	Phenomenex	00B-4435-B0
6520 Q-ToF mass spectrometer	Agilent	N/A
Agilent 1290 Infinity II UPLC	Agilent	www.agilent.com/ko-kr/product/liquid-chromatography/hplc-systems/analytical-hplc-systems

EXPERIMENTAL MODEL AND STUDY PARTICIPANT DETAILS

All bacteria and culture conditions used in this study can be found in the 'METHOD DETAILS' section. The strains used in this study are stored as glycerol stocks and lyophilized stocks.

METHOD DETAILS

Bacterial growth and culture conditions

E. callanderi KIST612 (=KCTC13263BP) was cultured in HEPES-buffered basal medium (HBBM) containing 20 mM glucose, gaseous CO (99.95% purity; Daedeok Gas Co., South Korea), and H_2/CO_2 mixture (80:20 [v/v]; Daedeok Gas Co.) as three different carbon and energy sources, respectively, as previously described [13,27]. For the ^{13}C isotope-labeling experiments, KIST612-derived strains were cultured in HBBM with CO and 30 mM [1,2-$^{13}C_2$] sodium acetate. Erythromycin (120 μg ml^{-1}) or chloramphenicol (50 μg ml^{-1}) was used for the selection of transformants or CoAT-double knockout mutants, respectively. For cultivation of Ca_AdhE1, Ca_AdhE2, and KIST612, all strains were cultured using 60 ml of HBBM in158-ml serum bottles. Before starting the culture, 101.3 kPa of gaseous CO was injected in the headspace of serum bottles. The CO (mmol) present in the headspace of the serum bottle was monitored over time, and additional CO was injected when its level fell below 1 mmol.

Plasmid and strain construction

All strains, plasmids, and primers used in this study are listed in Table S5 in the supplemental information online. To obtain recombinant CoA transferase (CoAT) and acetate kinase (Ack) proteins, DNA fragments containing each of the three putative genes coding for CoAT (ELI_2854, ELI_3452, and ELI_3772) and Ack (ELI_2893) were amplified using the individual primers in polymerase chain reactions (PCR) with the genomic DNA of KIST612 as a template. Each amplified DNA fragment contained two different restriction enzyme sites in the multiple cloning site of the pET-28a(+) vector at both the 5′- and the 3'-ends. Each DNA fragment and vector were treated with restriction enzymes (NEB; Ipswich, MA, USA), *Xho*I/*Nco*I, *Xho*I/*Nde*I, and *Ned*I/*BamH*I, respectively, according to the manufacturer's protocol.

To develop CoAT-knockout mutants, homologous arms-containing plasmids, pELMKO-2854HA, pELMKO-3452HA, pECas9-cat2, and pECas9-cat3, were constructed. pELMKO-2854HA and pELMKO-3452HA included the chloramphenicol resistance gene (*catP*) between both homologous arm sequences for CoAT-double knockout. The fragments containing homologous arms and *catP* were synthesized from Integrated DNA Technologies, Inc. (Coralville, IA, USA) and were introduced into pELMKO or pECas9 using SpeI site [20,28]. The plasmids for pELMKO-2854HA or pELMKO-3452HA were introduced into *E. callanderi ΔELI_3452* or *E. callanderi ΔELI_3772* after plasmid curing.

Two gene fragments were used to construct pECPH2::*adhE1* and pECPH2::*adhE2*. A gene fragment containing a pIP404 replicon and pMBI replicon with Erm^R was used as a backbone vector [27]. For the insert DNA fragment, the fragment, containing the gentamicin cassette and bifunctional aldehyde/alcohol dehydrogenase (CAETHG_3747 and CAETHG_3748) with H2 (P_{rbo}) as a strong promoter [27], was obtained using FW_AdhEwGmR and RV_AdhEwGmR primer sets and overlapping PCR. The gentamycin-resistant cassette was used for *E. coli* selection and amplified using FW_GmR and RV_GmR. The GmR cassette is linked to the 3′ end of the AdhE block gene fragment. Inserts and backbone DNA fragments were treated with *Spe*I and *Bmt*I restriction enzymes.

The digested fragments were ligated using T4 DNA ligase (Takara, Shiga, Japan) overnight at 16°C. *E. coli* HST04 (Takara) competent cells were used to construct plasmids. The transformant was selected on Lysogeny Broth agar plates including appropriate antibiotics (50 μg ml^{-1} kanamycin, 50 μg ml^{-1} gentamicin, 300 μg ml^{-1} erythromycin), and was confirmed using colony PCR or the digested fragment size using restriction enzyme sites. Successful cloning was confirmed by DNA sequencing (SolGent, Daejeon, South Korea) of each amplified insert DNA fragment including the promoter region. Transformation of the vectors into *E. callanderi* KIST612 competent cells was conducted using electroporation according to a previous study [27].

Enzyme assay

To prepare the cell-free crude extracts, 101.3 kPa of CO- or 20 mM glucose-grown cells were harvested at the exponential phase. The cells were harvested using a previously described method [18]. To disrupt the cells, a sonicator probe was used at 21% amplitude and applied every 2 sec for every 9 sec off at 4°C for 2 min. The cell-free crude extracts were collected anaerobically in a glove box (Coy Lab., Michigan, USA).

The recombinant pET vectors containing CoAT- and Ack-coding genes were heterologously expressed into *E. coli* BL21(DE3) competent cells. The cells were harvested after induction with isopropyl β-d-1-thiogalactopyranoside (IPTG) overnight at 16°C and using a shaking incubator at 180 rpm. The cell pellets were washed with 50 mM Tris-HCl buffer (pH 8.0, addition with 200 mM NaCl, 5% glycerol). Washed cell pellets were suspended in Tris-HCl buffer with one tablet of the complete EDTA-free protease inhibitor cocktail (Roche Molecular Biochemicals, IN, USA). Cells were disrupted using a sonicator (Vivra Cell Sonifier; Sonics and Materials Inc., USA) with the amplitude of the sonicator probe set at 35% on the pulse mode (pulse duration, 2 sec; rest duration, 9 sec) for 3 min at 4°C. The cell debris was removed, and His-tag purification was performed by slightly modifying the manufacturer's protocol for Ni-NTA agarose beads (Qiagen, Hilen, Germany). The mixture of supernatant and Ni-NTA beads was loaded onto the Ni-NTA column, and the column flow-through was collected. His-tagged proteins were eluted by increasing the imidazole concentration. Dialysis was performed using fractions showing the best purification with Tris-HCl buffer containing 1 mM DTT overnight at 4°C for desalting imidazole from the samples.

All enzyme assays were conducted anaerobically at 37°C in a 1.4-ml cuvette (114-QS; Hellma Analytics, Mulheim, Germany). Total protein was determined using the Bradford assay using Bio-Rad Protein Assay Dye (Bio-Rad, CA, USA) and bovine serum albumin

as a standard [29]. Fatty acid kinase enzyme activities were determined in cell-free extracts of *E. callanderi* KIST612 based on the NADH oxidation rate using pyruvate kinase and lactate dehydrogenase. The assay mixtures contained 1.7 mM phosphoenolpyruvate, 4.2 mM ATP, 0.4 mM NADH, pyruvate kinase (10 mg ml^{-1}), L-lactate dehydrogenase (10 mg ml^{-1}), 4.2 mM $MgCl_2$, and 100 mM Tris-HCl buffer (pH 7.6), 0.85 M sodium acetate or sodium butyrate [30]. The initial rates were determined at a wavelength of 340 nm (ε_{NADH} = 6.2 mM^{-1} cm^{-1}). The butyryl-CoA:acetate CoAT assay was used to measure the absorbance change of 5,5′-dithio-bis-2-nitrobenzoate (DTNB) [31]. The enzymatic activities were measured in 10 mM HEPES buffer (pH 7.0) containing 200 mM sodium acetate, 0.1 mM butyryl-CoA, 0.5 mM oxaloacetate, 2 μL citrate synthase (cat. #C3260; Sigma-Aldrich, St. Louis, MO, USA), and 0.5 mM DTNB. To determine the acetate/butyrate kinase for recombinant Ack (ELI_2893) protein, a hydroxamate assay detecting acetyl-phosphate/butyryl-phosphate formation was performed [32]. A reaction mixture was prepared by combining 333 μL of a solution containing 145 mM Tris-HCl (pH 7.4), 200 mM potassium acetate or potassium butyrate, 10 mM $MgCl_2$, 10 mM ATP, and 705 mM hydroxylamine hydrochloride (neutralized with KOH), with the indicated amounts of acetate kinase and incubating the mixture at 37°C for 12 min. To stop the reaction, 333 μL of a 10% trichloroacetic acid solution was promptly added. This was followed by adding 333 μL of 2.5% $FeCl_3$ (dissolved in 2.0 N HCl, yellow) to the reaction mixture. The composite mixture was incubated at room temperature for 5 min for color development (brown), and the absorbance was measured at 540 nm (ε = 0.47 mM^{-1} cm^{-1}) wavelength.

Regarding the enzyme assay for ethanol formation, the assay mixtures were modified from the previous method [16]. For measurement of the specific activity of alcohol dehydrogenase, the assay mixtures included 100 mM Tris-HCl (pH 7.5), 2 mM dithiothreitol (DTT), 50 mM ethanol, and 7.5 mM NAD^+. The assay mixture for the measurement of acetaldehyde dehydrogenase activity contained 100 mM Tris-HCl (pH 7.5), 2 mM DTT, 5 mM acetaldehyde, 2 mM coenzyme A, and 7.5 mM NAD^+. After the start of the reaction with the enzyme, the reduction of NAD^+ was monitored spectrophotometrically at 340 nm (ε = 6.2 mM^{-1} cm^{-1}). Acetaldehyde:Fd oxidoreductase (AOR) enzyme activity was monitored for optical density changes by methyl viologen (MV) reduction at 578 nm (ε_{MV} = 13.1 mM^{-1} cm^{-1}) [33]. The reaction mixture included 50 mM Tris-HCl buffer (pH 8.0), 4 mM MV, 2 mM acetaldehyde, and cell-free crude extract. The reaction was started by adding acetaldehyde. AOR enzyme activity was also monitored using Fd obtained from *C. pasteurianum* during laboratory preparation according to a previous report [34].

OMICS analyses

The KIST612 strain-derived cells were harvested at the mid-exponential and ES growth phases from each of the three different substrates (glucose, H_2 or CO) conditions for transcriptome analysis. Data for the selection of promoters were shared with Jeong and colleagues [27], and RNA sequencing and transcriptome data analysis were performed as described by these authors.

For proteome analysis, KIST612 strain-derived cells were harvested from the ES growth phase for each substrate condition (glucose or CO) to acquire samples. Sample preparation and data analysis were performed according to a previously described method [20]. Peptide samples were analyzed using a Q Exactive Plus Mass Spectrometer (Thermo Fisher Scientific, Bremen, Germany) in line with the Dionex Ultimate 3000 Nano-HPLC System. Peptides were separated using a two-column system with a trap column (2 cm × 75 μm Acclaim Pepmap 100 column) and an analytical column (15 cm × 75 μm Acclaim Pepmap RSLC C18 column). The instrumental conditions were in accordance with those from a previous study [20]. The data analysis was conducted according to a method validated in a previous study [20].

Instrumental analyses

Cell growth was determined based on optical density at 600 nm using a UV-Vis spectrophotometer (Jasco, Tokyo, Japan). The pH was measured using a pH meter (780 pH meter, Metrohm, Herisau, Switzerland). Glucose consumption was detected using a high-performance liquid chromatography system (HPLC, Younglin, South Korea) equipped with a refractive index detector and an Aminex HPX-87H column (Bio-Rad). The temperature of the column was maintained at 60°C and the flow rate of the mobile phase (5 mM H_2SO_4) was 0.6 ml min^{-1}. The gaseous CO and CO_2 in headspace of the serum bottles were measured using a gas chromatograph (ACME6100 GC, Younglin) equipped with a thermal conductivity detector (TCD) and carbon molecular sieve column (Carboxen 1000 with 60–80 mesh, Supelco, USA). The initial temperature of the oven was 105°C and it was steadily increased to 200°C at a rate of 30°C min^{-1}. H_2 gas was measured using a gas chromatograph (ACME6000, Younglin) equipped with a TCD and stainless steel packed with 100/120 mesh HayeSep D (Hayes Separation, Bandera, TX, USA). The temperature of the injector and detector was set to 150°C, and the flow rates of the N_2 carrier gas and reference gas were 20 ml min^{-1} and 30 ml min^{-1}, respectively.

Fatty acids (acetate, butyrate) and alcohols (ethanol, butanol) were measured using GC (ACME 6100) equipped with a flame ionization detector (FID) and a capillary column (AquaWax, Alltech, USA). The temperature of the injector and detector was set to 250°C. The flow rate of the N_2 carrier gas was 2.0 ml min^{-1}. For GC-FID operation, the oven temperature was increased steadily from 55°C to 200°C at a rate of 12°C min^{-1}. The centrifuged and filtered sample was acidified by adding 1 M phosphoric acid, and hexanoic acid was used as an internal standard.

Gas chromatography combustion isotope ratio mass spectrometry (GC-C-IRMS) was used for ^{13}C isotope enrichment analysis. The ^{13}C ratio of whole samples was diluted such that the ^{13}C enrichment percentage of the samples did not exceed 6% to obtain accurate results without exceeding the detection limit of IRMS. First, all samples were diluted to 1/100. Based on the maximum concentration of the metabolites acetate, ethanol, butyrate, and butanol (analyzed previously using GC-FID), a mixture of ^{12}C-based normal metabolites (final concentration: 4 mM acetate; 4 mM ethanol, 2 mM butyrate, 1 mM butanol) was then prepared and mixed with each sample to provide an internal standard, and to lower the ^{13}C percentage of each metabolite in the diluted samples artificially (^{13}C ratio for each metabolite in the sample did not exceed the maximum of 6%). The ^{13}C ratio of the prepared samples was determined using GC-C-IRMS. An IRMS instrument (Isoprime, Cheadle, UK) was connected to a Hewlett Packard 7890N series GC (Agilent Technologies, Santa Clara, USA) *via* a combustion interface (glass tube packed with copper oxide, operated at 850°C). A capillary column (AquaWax; Alltech) was used with He (at a constant flow rate of 2.0 mg ml^{-1}) as the carrier gas. Samples were injected using the same temperature program used for the GC-FID analysis. Reference CO_2 gas of known $\delta^{13}C$ values was pulsed at the beginning and end of each sample run. Standard carbon isotope ratios were expressed as $\delta^{13}C$ values per milliliter relative to Vienna Pee Dee Belemnite. To monitor the accuracy of the measurements, standards with known $\delta^{13}C$ values were analyzed every 5–6 sample runs. Standard deviations of carbon isotope measurements were of the order ±0.1 as determined by repeated injections of the standard.

For detection of [1,2-$^{13}C_2$] acetyl phosphate and [1,2-$^{13}C_2$] acetyl-CoA as intracellular metabolites in the *E. callanderi* strain, an LC-MS/MS analysis was performed on a Shimadzu LC-40 system with AB SCIEX 4500 Q-Trap with the Gemini C18 column (50 mm × 2.0 mm, 5 µm). For the mobile phase, eluents A and B were 10 mM ammonium formate and acetonitrile, respectively. The gradient was as follows: 10% B at 0 min, 65% B at 2 min, and 10% B at 3.1 min with a 0.3 ml min^{-1} flow rate. The MS system was operated under a turbo ion spray mode. The source was set at 4.5 kV ion spray voltage, curtain gas at 35 psi, nebulizer gas at 50 psi, and heater gas at 50 psi. Acetyl phosphate and [1,2-$^{13}C_2$] acetyl phosphate were synthesized using a previously reported method [35,36] and validated (Figure S4 in the supplemental information online). For validation of synthetic acetyl phosphate and [1,2-$^{13}C_2$] acetyl phosphate, LC-MS/MS analysis was performed on Liquid and Gas Chromatography Ultra high-resolution Quadrupole Time of Flight Mass Spectrometer System (Agilent 1290 Infinity II UPLC) with a ZIC-pHILIC polymeric bead, poly(ether-ether-ketone) (PEEK)-coated column (100 × 2.1 mm, 5 µm; Merck KGaA) at 35°C. For the mobile phase, A and B were distilled water plus 10 mM ammonium carbonate and acetonitrile, respectively. The linear gradient was as follows: 80% B at 0 min, 35% B at 10 min, 5% B at 12 min, 5% B at 25 min, 80% B at 25.1 min, and 80% B at 45 min, with a 0.15 ml min^{-1} flow rate. MS data were acquired using a 6520 Q-ToF mass spectrometer (Agilent) equipped with an electrospray ionization source. The multiple reaction monitoring transitions of the parent ion to fragment ions, 139>79 m/z for ^{12}C-acetyl phosphate, 141>79 m/z or 141>63 m/z for $^{13}C_2$-acetyl phosphate, 808>408 m/z for ^{12}C-acetyl-CoA, and 810>408 m/z for $^{13}C_2$-acetyl-CoA were monitored in the negative detection mode. To extract intracellular metabolites, cells were quenched at a ratio of methanol:acetonitrile:distilled water = 2:2:1, and disrupted using a sonicator. All samples were prepared by dilution and 244 ng ml^{-1} propionyl-CoA was added for metabolite quantification. To quantify each metabolite, acetyl phosphate, [1,2-$^{13}C_2$] acetyl phosphate, acetyl-CoA, and [1,2-$^{13}C_2$] acetyl-CoA were used as standard chemicals and propionyl-CoA as an internal standard. The data were obtained and the average and standard deviation calculated using duplicate samples to ensure accuracy and reproducibility.

QUANTIFICATION AND STATISTICAL ANALYSIS

Data are shown as means ± standard deviation (SD). Sample size is indicated in figure legends. All statistical analyses were performed using R (version 4.2.3.) and RStudio (version 2023.03.0+386) software. Significant differences are presented in figures using * $P<0.05$, ** $P<0.01$, and *** $P<0.001$.